Electronic Supplementary Material (ESI) for Journal of Materials Chemistry C.

Supplementary Information

Highly Conductive PEDOT:PSS Fibers for Applications in Electronic Textiles

Ruben Sarabia-Riquelme, Rodney Andrews, John E. Anthony, and Matthew C. Weisenberger*

Immersion tests in sulfuric acid

PTFE spools with raw fibers wound on them were immersed in 93 wt.% sulfuric acid such that all the fibers were covered with the sulfuric acid solution. The fibers were left immersed for different periods of time (1, 5, 10, 30 and 60 min) at room temperature. Then, they were transferred to a large deionized water bath where they were left immersed for 10 min in order to wash off the sulfuric acid from the fibers. Lastly, the washed spools where transferred to an oven where they were dried at 140 ºC for 10 min. **Figure S1**a and b show the change in diameter and linear density, respectively, versus immersion time in the sulfuric acid bath for two raw fiber samples at total draws of 1.58 and 3.34. In both cases, after only one minute of treatment, a sharp reduction in diameter and linear density was observed, followed by a rather constant trend. The electrical conductivity of these sulfuric acid immersed fibers is shown in Figure S1c. For both samples, the electrical conductivity increased with increasing treatment time until it saturated after 30 min of treatment at values around 3200-3500 S cm^{-1}.

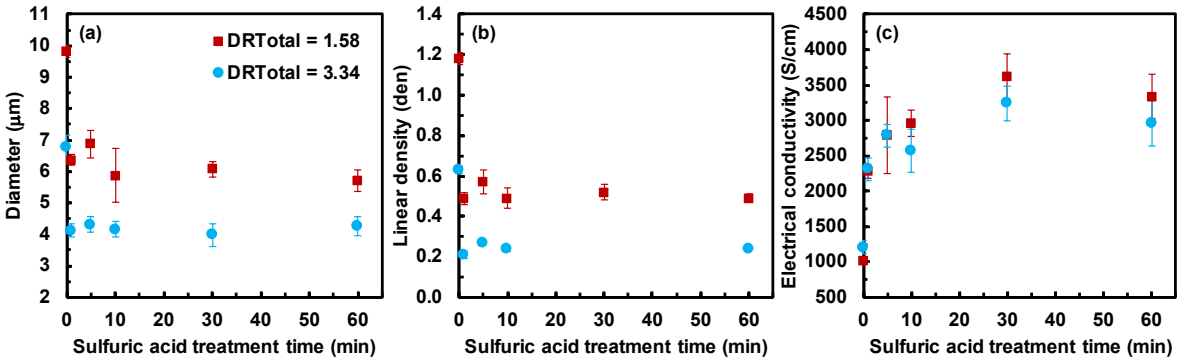

Figure S1. (a) Diameter, (b) linear density, and (c) electrical conductivity as a function of sulfuric acid immersion treatment time.

Wet-spinning process with a sulfuric acid drawing step

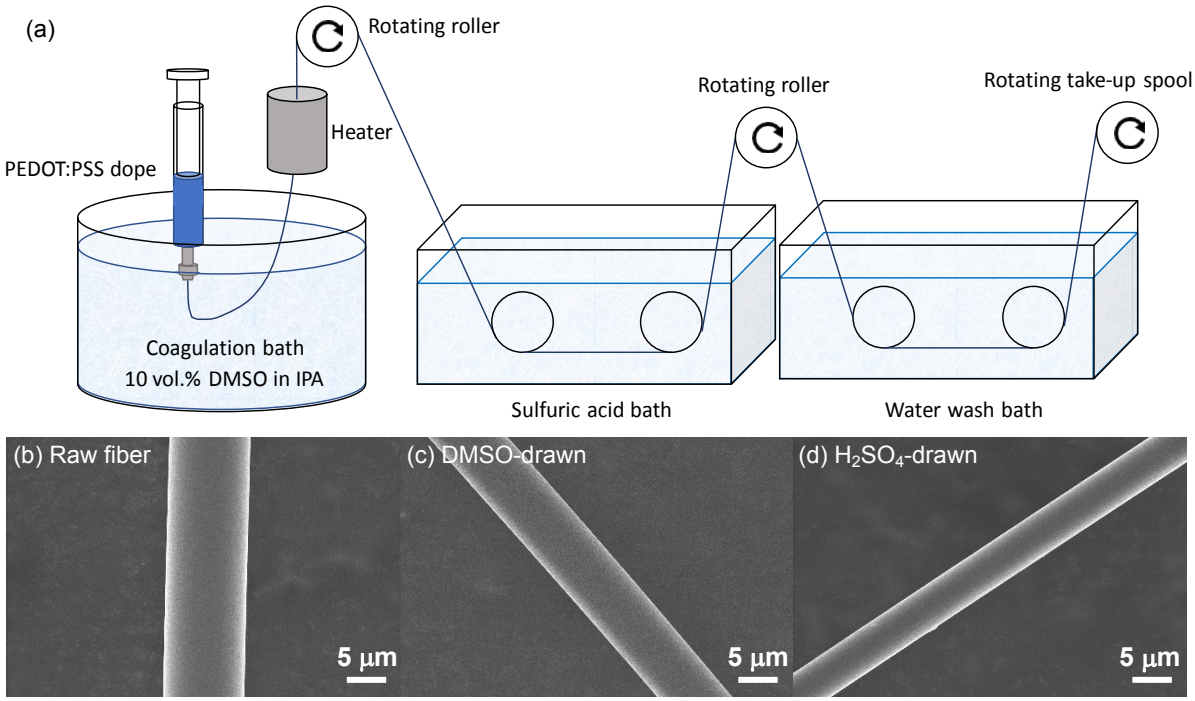

Figure S2. (a) Schematic of the PEDOT:PSS wet-spinning process including a sulfuric acid draw bath. SEM images of (b) raw fiber, (c) DMSO-drawn fiber, and (d) H_2SO_4-drawn fiber.

Calculation of the linear density of the fibers from the mass balance equation

The linear density of the fibers can be found by applying a mass balance to the wet-spinning system with respect to PEDOT:

$$\dot{M}_{PEDOT,\,dope} = \dot{M}_{PEDOT,\,washed} + \dot{M}_{PEDOT,\,fiber} \qquad \text{eq. S1}$$

where $\dot{M}_{PEDOT,\,dope}$ is the mass flow of PEDOT entering the coagulation bath from the syringe, $\dot{M}_{PEDOT,\,washed}$ is the mass flow of PEDOT being washed off in the DMSO or sulfuric acid baths and $\dot{M}_{PEDOT,\,fiber}$ is the mass flow of PEDOT being taken up as a fiber. We will assume that only PSS is being washed off in the DMSO or sulfuric acid baths and, thus, $\dot{M}_{PEDOT,\,washed} = 0$. Additionally, for $\dot{M}_{PEDOT,\,dope}$ and $\dot{M}_{PEDOT,\,fiber}$ we have:

$$\dot{M}_{PEDOT,\,dope} = \dot{Q}\cdot\rho_{dope}\cdot C_{PEDOT:PSS,dope}\cdot wt.\%\ PEDOT_{dope} \qquad \text{eq. S2}$$

$$\dot{M}_{PEDOT,\,fiber} = LD\cdot v_{take-up}\cdot wt.\%\ PEDOT_{fiber} \qquad \text{eq. S3}$$

where $\dot{Q}$ is the volumetric flow rate (constant at 0.25 mL/h), ρ_{dope} is the dope density (assumed to be ~ 1 g/cm^3), $C_{PEDOT:PSS,dope}$ is the concentration of PEDOT:PSS in the dope (2.5 wt.% in this work) and $wt.\%\ PEDOT_i$ is the weight percentage of PEDOT with respect to PSS (28.57 wt.% for the dope). Using equation S1, S2 and S3, the linear density can be expressed as:

$$LD = \frac{A_{spinneret} \cdot \rho_{dope} \cdot C_{PEDOT:PSS,dope}}{DR_{Total}} \frac{wt.\%\ PEDOT_{dope}}{wt.\%\ PEDOT_{fiber}} \qquad \text{eq. S4}$$

where $A_{spinneret}$ is the cross-sectional area of the spinneret orifice and DR_{Total} is the total draw calculated as the ratio between take-up speed and dope speed. Using equation S4, the linear density of the fibers can be calculated as a function of total draw for a given weight percentage of PEDOT in the final fiber.

Calculation of crystallite size

The crystallite size along the a and b directions was calculated using the Scherrer's equation:

$$L_Z = \frac{K\lambda}{\beta cos\theta} \qquad \text{eq. S5}$$

where L_Z is the crystallite size along a direction *Z*, *K* is a dimensionless shape factor (value of 0.9 used in this work), λ is the X-ray wavelength (1.54 Å in this work) and β is the full width at half maximum (FWHM) of the corresponding peak in radians.

Calculation of the degree of crystallinity

The degree of crystallinity, χ_c, was calculated for the different samples. For this purpose, the (100) and (020) peaks in 2D WAXS patterns were considered as the signal for the crystalline regions, while the peak corresponding to the PSS halo was considered amorphous signal. χ_c was then calculated using the following equation:

$$\chi_c = \frac{A_{(100)} + A_{(020)}}{A_{(100)} + A_{(020)} + A_{PSS}} \cdot 100 \qquad \text{eq. S6}$$

where A_Z is the area of the 2D WAXS peak corresponding to the *Z* reflection.

Calculation of Hermans orientation factors

To quantify the degree of orientation of the fibers, the Hermans orientation factor, f_c, was calculated from the WAXS data using

$$\left\langle \cos^2 \Psi_{c,Z} \right\rangle = \frac{\int_0^{\pi} I(\Psi) \sin \Psi \cos^2 \Psi d\Psi}{\int_0^{\pi} I(\Psi) \sin \Psi d\Psi} \qquad \text{eq. S7}$$

and

$$f_c = \frac{3\left\langle \cos^2 \Psi_{c,Z} \right\rangle - 1}{2} \qquad \text{eq. S8}$$

In these equations, Ψ is the azimuthal angle, $I(\Psi)$ represents the azimuthal intensities, and $\left\langle \cos^2 \Psi_{c,Z} \right\rangle$ is the average cosine square of the angle that the c-plane made with the draw direction, Z. f_c takes values of 0 for an isotropic material with no preferred orientation, -0.5 when the crystal planes are oriented perpendicular to the draw direction, and 1 for fully oriented planes parallel to the draw direction.

Ampacity of the PEDOT:PSS fibers

Figure S3a shows the resistance divided by the initial resistance, R/R_0, as a function of current density for raw fiber samples. To obtain these curves, fiber specimens were mounted in 2-probe configuration and the voltage was swept at rates between 0.1 mV s^{-1} to 1000 mV s^{-1} while measuring the current until electrical failure of the fiber occurred. The resistance of the fiber at each *I-V* point was then calculated using Ohm's law. The maximum current density value of each of the curves corresponds to the value at electrical failure. This was observed as a steep onset in resistance increase, then the fiber's resistance increased irreversibly until breakdown. As can be observed, the value of maximum current density depended on the voltage sweep rate. At high sweep rates, the maximum current was achieved in a short period of time (< 3 s), and the process largely occurred with the fiber not being at thermal equilibrium. At low sweep rate,

the maximum current was achieved in a long period of time (> 5 h) and the fiber can be largely considered to be at thermal equilibrium at each given point. An ampacity of 16.2 kA cm^{-2} can be extracted from the 1000 mV s^{-1} curve but it is only valid for peaks of current that last very short period of times (< 3 s). A more practical value of 11.3 kA cm^{-2} can be extracted from the 0.1 mV s^{-1} curve, which is valid for continuous operation. Indeed, Figure S3b shows the change in resistance with time of raw fiber specimens kept at a certain current density for 60 min. The fibers kept at 12 kA cm^{-2} and 11.5 kA cm^{-2} broke after 7.4 min and 56.4 min of operation, respectively, while the fiber kept at 11 kA cm^{-2} did not break. This suggested that the ampacity for continuous operation is between 11 and 11.5 kA cm^{-2}, which is in good agreement with the value of 11.3 kA cm^{-2} obtained from Figure S3a at a voltage sweep rate of 0.1 mV s^{-1}. Similar R/R_0 versus current density curves at different voltage sweep rates were obtained for DMSO-drawn fibers and H_2SO_4-drawn fibers. Figure S3c shows the values of ampacity for the three types of fiber as a function of the voltage sweep rate. As can be observed the DMSO-drawn fibers have higher values of ampacity than the coagulation bath fibers. Nevertheless, the highest values of ampacity are found for H_2SO_4-drawn fibers.

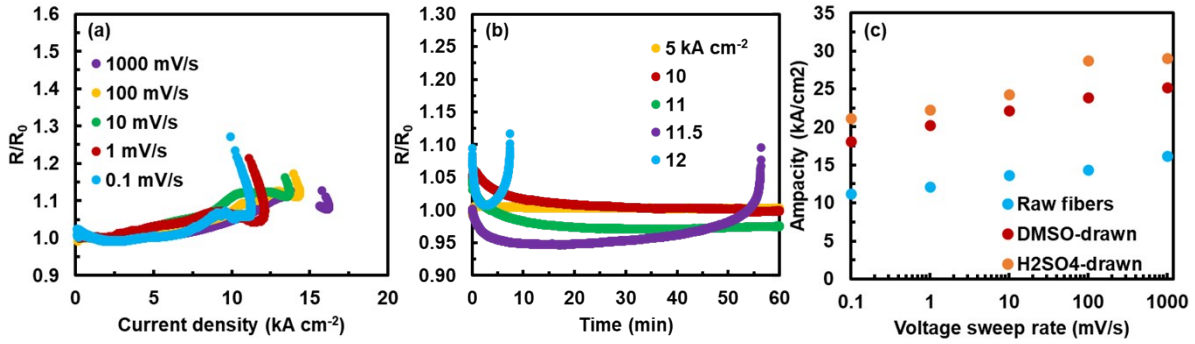

Figure S3. (a) Resistance (standardized to the initial resistance) of raw fibers versus current density at different voltage sweep rates until electrical failure. (b) Change in resistance (standardized to the initial resistance) of raw fibers with time at different constant current densities. (b) Ampacity as a function of the voltage sweep rate for the different types of fiber.

Joule heating characteristics of DMSO-drawn PEDOT:PSS fibers

An infrared camera (FLIR i60) was used to record videos of DMSO-drawn fiber specimens while passing current through them, and temperature versus time plots were generated. **Figure S4**a shows the temperature of the fiber versus time while the current was increased in steps of 0.5 mA each 30 seconds until the electrical failure of the fiber occurred. The temperature of the fiber reached approximately 80 ºC before thermal runaway occurred followed by electrical failure. The temperature of the fiber increased parabolically with the current density as shown in Figure S4b. It must be noted that the temperature here referred as "temperature of the fiber" is the temperature as obtained from the infrared camera. However, the resolution of the camera was not sufficient to properly capture the single filaments due to their small diameter. To work around this, the fibers were mounted on paper substrates with low thermal conductivity. The temperature recorded is, therefore, the temperature of the area around the contact between the fiber and paper. The actual temperature of the fiber is unknown and likely to be higher.

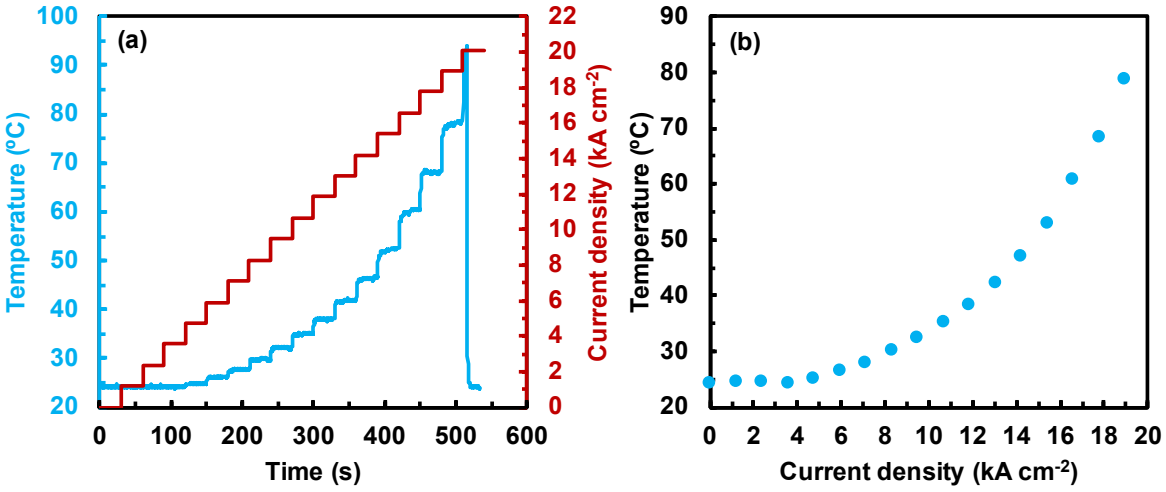

Figure S4. (a) Temperature of a fiber versus time while increasing the current by 0.5 mA each 30 s. (b) Temperature of the fibers as a function of the current density.

Calculation of the output characteristics of a thermoelectric generator

A thermoelectric generator is composed of several thermoelectric couples, which are made of n-type and p-type legs connected electrically in series but thermally in parallel (**Figure S5**a). A

thermoelectric generator can be modelled as a voltage source connected in series with a resistor that represents the internal resistance of the device, R_i, as shown in Figure S5b.

Ohm's law applied to the circuit in Figure S5b gives:

$$V_{OC} = I(R_i + R_L) \qquad \text{eq. S9}$$

where V_{OC} is the open circuit voltage, I is the current and R_L is the load resistance.

V_{OC} is simply the thermoelectric voltage produced due to the temperature difference, ΔT:

$$V_{OC} = N(\alpha_p - \alpha_n)\Delta T \qquad \text{eq. S10}$$

where N is the number of couples connected in series in the device and α_p and α_n are the Seebeck coefficients of the p and n-type materials, respectively.

The short circuit current, I_{SC}, can be extracted from equation S9 by simply substituting $R_L = 0$.

$$I_{SC} = \frac{V_{OC}}{R_i} \qquad \text{eq. S11}$$

The electrical power, P, delivered to the load is given by:

$$P = I^2 R_L = \frac{{V_{OC}}^2 R_L}{(R_i + R_L)^2} \qquad \text{eq. S12}$$

The maximum power, P_{max}, from equation S12 is obtained when the load resistance matches the internal resistance of the thermoelectric generator ($R_L = R_i$) and can be written in terms of V_{OC} and I_{SC}:

$$P_{max} = \frac{{V_{OC}}^2}{4R_i} = \frac{{I_{SC}}^2 R_i}{4} = \frac{V_{OC} I_{SC}}{4} \qquad \text{eq. S13}$$

Equation S13 provides a very interesting result since it basically states that to characterize the maximum power output of a thermoelectric device at any given temperature only two measurements are needed (any pair between V_{OC}, I_{SC} and R_i).

Moreover, using equation S10 and S13, we can express the maximum output power as a function of the thermoelectric properties of the p and n-type materials, the geometry of the device and the temperature difference as follows:

$$P_{max} = \frac{NA}{4L} \cdot \frac{(\alpha_p - \alpha_n)^2}{\left(\frac{1}{\sigma_p} - \frac{1}{\sigma_n}\right)} \Delta T^2 \qquad \text{eq. S14}$$

where it has been assumed that both p and n-type legs have the same length, L, and cross-sectional area, A. To obtain equation S14 the definition of electrical conductivity, $\sigma = L/RA$, has been used.

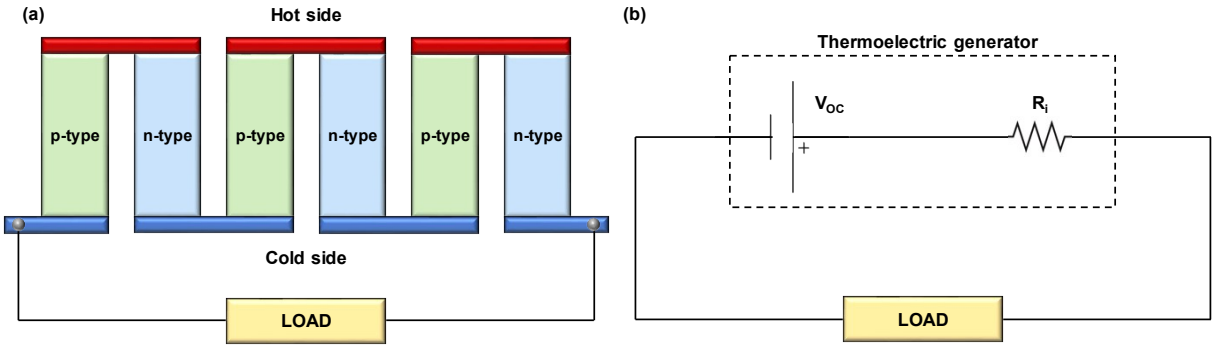

Figure S5. (a) Scheme of a thermoelectric generator showing p-n couples connected electrically in series but thermally in parallel. (b) Equivalent electrical circuit of a thermoelectric generator.

Several parameters from textile thermoelectric generators previously reported in the literature are listed in **Table S1**.

Table S1. Performance parameters of previously reported textile thermoelectric devices.

Materials		σ_p	$\alpha_p^2\sigma_p$	# of couples	ΔT	V_{OC}	P_{max}	Ref.
p-type	n-type	S cm^{-1}	μWK^{-2}m^{-1}		°C	mV	μW	
PEDOT:PSS coated nylon fibers	Ag_2Te nanocrystal films	-	-	4	20	3.5	0.005	1
PEDOT:PSS coated polyester fabric	Silver wires	3	0.05	5	75.2	4.3	0.012	2
PEDOT:PSS dyed silk yarns	Silver wires	14	0.32	26	66	20.4	0.012	3
PEDOT:PSS dyed silk yarns	PVP/MWCNT coated PET yarns	14	0.32	38	80	98.4	0.007	4

PEDOT:PSS hydrogel fibers	PEI/SWCNT fibers	173	3.78	5	60	20.7	0.433	5
Wet-spun PEDOT:PSS fibers	Ag-plated nylon yarns	830	30	10	40	7.9	0.003	6
CNT/PVDF layers	CNT/PVDF layers	4.8	0.05	72	50	26	0.137	7
SDBS/CNT layers	PEI/CNT layers	110	103.5	72	32	150	1.800	8
CNT/PEDOT:PSS-Hydrazine fibers	CNT/PEDOT:PSS -Hydrazine fibers	1000	83.2	12	10	8	0.430	9
Wet-spun PEDOT:PSS fibers (DMSO-drawn)	Alumel wires	2244	40-50	20	84	45.9	2.820	This work

Transconductance of OECTs fabricated with PEDOT:PSS fibers acting as the channel

A scheme of an organic electrochemical transistor (OECT) is shown in **Figure S6**a. Figure S6b shows the transfer curves of the PEDOT:PSS fiber-based OECT. For a constant value of V_D, the drain current decreases as V_G increases, consistent with the behavior of a p-type depletion-mode OECT. The transduction efficiency is usually calculated using the first derivative of the transfer curves and it is called transconductance, g_m.[10]

$$g_m = \frac{\partial I_D}{\partial V_G} \qquad \text{eq. S15}$$

Per equation S15, if an OECT has a large transconductance, small changes in the gate voltage will result in large changes in the drain current, effectively amplifying the input signal. The transconductance of the PEDOT:PSS fiber-based OECT as a function of V_G at different constant V_D are presented in Figure S6c. The transconductance is higher at low values of V_G (good for amplifying small signals) while operating near the saturation regime (V_D = -0.6 V). The transconductance can be increased by fabricating OECTs with more fibers connected in parallel acting as the channel. Figure S6d shows the transconductance curves as a function of V_G and at constant V_D = -0.6 V for OECTs fabricated using 1, 2, 5 and 10 fibers as channel. A linear relationship between the transconductance and the number of fibers acting as the channel can be observed in Figure S6e where the maximum transconductance (at V_D= -0.6 V and V_G= 0.2

V) of the PEDOT:PSS fiber-based OECTs is plotted against the number of fibers acting as the channel. In these devices the channel length was kept constant at 1 cm.

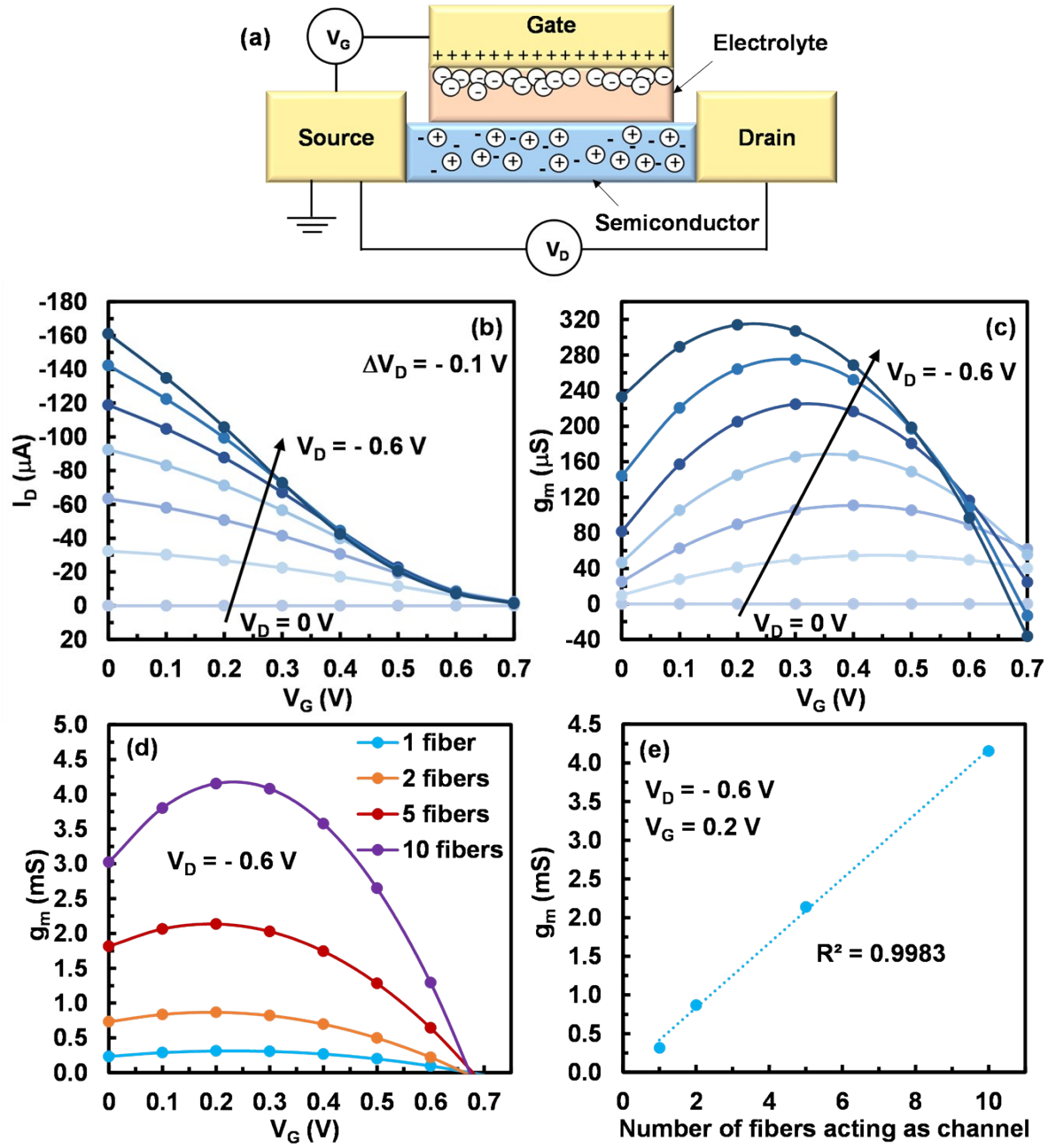

Figure S6. (a) Scheme of an organic electrochemical transistor. (b) Transfer curves showing the dependence of I_D on V_G. (c) Transconductance as a function of V_G. Both (b) and (c) at different values of V_D from 0 V to -0.6 V with ΔV_D of -0.1 V and channel length of 1 cm. (d) Transconductance as a function of V_G at V_D = -0.6 V for OECTs with different number of fibers acting as the channel (with 1 cm length). Solid lines connecting the data points are guides to

the eye. (e) Transconductance at V_D = -0.6 V and V_G = 0.2 V as a function of the number of fibers acting as the channel (1 cm) showing the linear relationship between these two parameters.

References for Supplementary Information

1. S. W. Finefrock, X. Zhu, Y. Sun and Y. Wu, *Nanoscale*, 2015, **7**, 5598-5602.
2. Y. Du, K. Cai, S. Chen, H. Wang, S. Z. Shen, R. Donelson and T. Lin, *Scientific Reports*, 2015, **5**, 6411.
3. J. D. Ryan, D. A. Mengistie, R. Gabrielsson, A. Lund and C. Müller, *ACS Applied Materials & Interfaces*, 2017, **9**, 9045-9050.
4. J. D. Ryan, A. Lund, A. I. Hofmann, R. Kroon, R. Sarabia-Riquelme, M. C. Weisenberger and C. Müller, *ACS Applied Energy Materials*, 2018, **1**, 2934-2941.
5. J. Liu, Y. Jia, Q. Jiang, F. Jiang, C. Li, X. Wang, P. Liu, P. Liu, F. Hu, Y. Du and J. Xu, *ACS Applied Materials & Interfaces*, 2018, **10**, 44033-44040.
6. Y. Kim, A. Lund, H. Noh, A. I. Hofmann, M. Craighero, S. Darabi, S. Zokaei, J. I. Park, M.-H. Yoon and C. Müller, *Macromolecular Materials and Engineering*, 2020, **305**, 1900749.
7. C. A. Hewitt, A. B. Kaiser, S. Roth, M. Craps, R. Czerw and D. L. Carroll, *Nano Letters*, 2012, **12**, 1307-1310.
8. S. L. Kim, K. Choi, A. Tazebay and C. Yu, *ACS Nano*, 2014, **8**, 2377-2386.
9. J.-Y. Kim, W. Lee, Y. H. Kang, S. Y. Cho and K.-S. Jang, *Carbon*, 2018, **133**, 293-299.
10. J. Rivnay, S. Inal, A. Salleo, R. M. Owens, M. Berggren and G. G. Malliaras, *Nature Reviews Materials*, 2018, **3**, 17086.